Inorganic Chemistry
Cite This: Inorg. Chem. XXXX, XXX, XXX−XXX
Article
pubs.acs.org/IC

Observation of a Large Magnetic Anisotropy and a Field-Induced Magnetic State in $SrCo(VO_4)(OH)$: A Structure with a Quasi One-Dimensional Magnetic Chain

Liurukara D. Sanjeewa,*[,†,§] V. Ovidiu Garlea,[‡] Randy S. Fishman,[†] Michael A. McGuire,[†] Jie Xing,[†] Huibo Cao,[‡] Joseph W. Kolis,*[,§] and Athena S. Sefat[†]

[†]Materials Science and Technology Division, Oak Ridge National Laboratory, Oak Ridge, Tennessee 37831, United States
[‡]Neutron Scattering Division, Oak Ridge National Laboratory, Oak Ridge, Tennessee 37831, United States
[§]Department of Chemistry and Center for Optical Materials Science and Engineering Technologies (COMSET), Clemson University, Clemson, South Carolina 29634-0973, United States

Supporting Information

ABSTRACT: A new member of the descloizite family, a cobalt vanadate, $SrCo(VO_4)(OH)$, has been synthesized as large single crystals using high-temperature and high-pressure hydrothermal methods. $SrCo(VO_4)(OH)$ crystallizes in the orthorhombic crystal system in space group $P2_12_12_1$ with the following unit cell parameters: a = 6.0157(2) Å, b = 7.645(2) Å, c = 9.291(3) Å, V = 427.29(2) Å^3, and Z = 4. It contains one-dimensional Co−O−Co chains of edge-sharing CoO_6 octahedra along the a-axis connected to each other via VO_4 tetrahedra along the b-axis forming a three-dimensional structure. The magnetic susceptibility of $SrCo(VO_4)(OH)$ indicates an antiferromagnetic transition at 10 K as well as unusually large spin orbit coupling. Single-crystal magnetic measurements in all three main crystallographic directions displayed a significant anisotropy in both temperature- and field-dependent data. Single-crystal neutron diffraction at 4 K was used to characterize the magnetically ordered state. The Co^{2+} magnetic spins are arranged in a staggered configuration along the chain direction, with a canting angle that follows the tipping of the CoO_6 octahedra. The net magnetization along the chain direction, resulting in ferromagnetic coupling of the a-axis spin components in each chain, is compensated by an antiferromagnetic interaction between nearest neighbor chains. A metamagnetic transition appears in the isothermal magnetization data at 2 K along the chain direction, which seems to correspond to a co-alignment of the spin directions of the nearest neighbor chain. We propose a phenomenological spin Hamiltonian that describes the canted spin configuration of the ground state and the metamagnetic transition in $SrCo(VO_4)(OH)$.

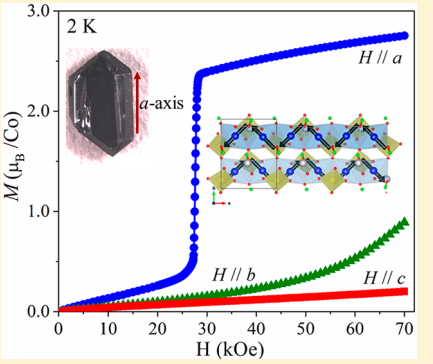

1. INTRODUCTION

Magnetic materials with one-dimensional (1D) chains built from edged sharing transition metal octahedra have attracted much attention due to their diverse exciting physical properties.[1−3] It is well-known that there are examples of crystals with no long-range magnetic ordering at the lowest observed temperatures in well-isolated 1D magnetic materials made from spin $^1/_2$ magnetic ions such as Cu^{2+} or V^{4+}.[4−9] A large number of 1D compounds display long-range ordering due to interchain interactions through nonmagnetic linking groups. Thus, most of the 1D compounds are categorized as pseudo-one-dimensional magnetic materials. The ordering temperatures of these pseudo-one-dimensional compounds largely depend on the spin state of the magnetic ions and the competition between intra- and interchain interactions in the structure. Additionally, the magnetic anisotropy could also lead to complex magnetic phase diagrams in this class of compounds, leading to interesting magnetic properties.[10−13]

Various mineral types with 1D magnetic chains are good candidates for such interesting magnetic phenomena.[14] The pyroxene class, for example, has been studied in considerable detail. Pyroxene has a common formula of AMX_2O_6 (A = Li or Na; M = Ti^{3+}, V^{3+}, Cr^{3+}, Mn^{3+}, or Fe^{3+}; X = Si^{4+} or Ge^{4+}). The general structure consists of 1D zigzag chains of edge-sharing MO_6, with the chains connected through XO_4 units to provide a quasi 1D magnetic structure. These compounds display extremely rich magnetic properties depending on the A-site cation and the transition metal cation. For example, Ti-based pyroxenes exhibit spin-Peierls-like transitions while V^{3+}-based pyroxenes are known to be perfect Haldane-chain compounds with S = 1 spin states.[15,16] A complete summary of pyroxene-type magnetic materials is given in ref 10. Brackebuschite is another mineral type that has been synthesized containing V^{3+}, Mn^{3+}, and Fe^{3+} ions, and their bulk magnetic properties have been characterized.[9] These compounds possess completely isolated 1D chains made from edge-sharing transition metal octahedra. Bulk magnetic measurements of $Ba_2V(VO_4)_2(OH)$

Received: August 12, 2019

DOI: 10.1021/acs.inorgchem.9b02427
Inorg. Chem. XXXX, XXX, XXX−XXX

(S = 1) reveal a broad maximum in magnetic susceptibility at ~100 K with no sign of magnetic ordering down to 2 K suggesting spin-liquid behavior.[9] On the other hand, brackebuschite-type $Pb_2Mn(VO_4)_2(OH)$ (S = 2) exhibits a ferromagnetic transition at T_C = 14 K.[17] Descloizite [Pb(Zn,Cu)$(VO_4)(OH)$] is another mineral type in which, in this case, divalent transition metal cations form the 1D chains compared to the more common trivalent transition metal cation chains in pyroxene and brackebuschite.[18,19] Recently, we have examined the bulk magnetic properties and magnetic structure of the descloizite-type $SrMn(VO_4)(OH)$ compound with $S = {}^5/_2$.[20] The magnetic study reveals a broad maximum at approximately 80 K in magnetic susceptibility before antiferromagnetic order at T_N = 30 K.[21] Single-crystal neutron diffraction of $SrMn(VO_4)(OH)$ revealed that Dzyaloshinskii–Moriya antisymmetric exchange interaction leads to slight spin canting that produces a weak ferromagnetism along the chain direction.

As discussed previously, mineral structures provide an excellent inspiration for investigating new materials with exciting magnetic properties.[13] Detailed magnetic measurement of naturally occurring minerals themselves is often complicated by the fact that the samples are usually contaminated with magnetic impurities such as iron, which mitigates their interesting magnetic properties. Therefore, a versatile synthetic method is essential for obtaining clean samples and large single crystals of mineral-based compounds. Consequently, we use a high-temperature high-pressure solution-based technique to access these mineralogically inspired magnetic materials and other interesting related low-dimensional magnetic materials.[14,22−25] Recently, we have been devoting our attention to transition metal vanadates. In contrast to phosphate (PO_4^{3-}) and arsenates (AsO_4^{3-}), vanadium can possess several oxidation states, including V^{3+} (S = 1) and V^{4+} ($S = {}^1/_2$) in addition to the nonmagnetic V^{5+}. Additionally, vanadium can form different oxy anions such as VO_4^{3-}, $V_2O_7^{4-}$, and VO_5^{2-}.[26−28] The vanadate (V^{5+}) building blocks are nonmagnetic, but the presence of empty d orbitals in the bridging group could modify the Goodenough–Kanamori–Anderson superexchange rules.[29]

This article focuses on descloizite-type $SrCo(VO_4)(OH)$ with edge-sharing chains of Co−O−Co made from $Co^{2+}O_6$ octahedra ($S = {}^3/_2$), and the Co−O−Co chains are interconnected with tetrahedral vanadate groups to provide a three-dimensional structure. Large single crystals of $SrCo(VO_4)(OH)$ were synthesized using a high-temperature hydrothermal method, and anisotropic magnetic properties were determined by magnetic susceptibility measurements. The magnetic structure was determined by single-crystal neutron diffraction. This compound exhibits a pronounced anisotropic behavior in its magnetic susceptibility, with a field-induced metamagnetic transition along the Co−O−Co chain direction (the a-axis). Interestingly, neutron diffraction confirms that the magnetic spins are arranged ferromagnetically along the chain direction but are antiferromagnetic between the chains.

2. EXPERIMENTAL SECTION

2.1. Hydrothermal Synthesis of $SrCo(VO_4)(OH)$. Hydrothermal crystal growth of $SrCo(VO_4)(OH)$ was performed using 2.75 in. silver tubing that had an inner diameter of 0.375 in. After silver tubes were welded shut on one side, the reactants and the mineralizer were added. The silver ampules were then welded shut and placed in a Tuttle-seal autoclave filled with water to provide appropriate counter pressure. The autoclaves were then heated to 580 °C for 10 days, reaching an average pressure of 1.7 kbar. Crystals were recovered by washing with deionized water. $SrCo(VO_4)(OH)$ single crystals were synthesized using a mixture of SrO, Co_3O_4, and V_2O_5 with a CsOH mineralizer. A typical reaction consisted of 0.4 g of total reactants (0.0788 g of SrO, 0.1830 g of Co_3O_4, and 0.1382 g of V_2O_5) in a stoichiometric ratio of 1:1:1 with 0.8 mL of 5 M CsOH. The single-crystal specimen of $SrCo(VO_4)(OH)$ in Figure 1a (4 mg) was used in both magnetic property characterizations and single-crystal neutron diffraction. The chemical reagents were used as received from the supplier: SrO (Alfa Aesar, 99.9%), Co_3O_4 (Alfa Aesar, 99.9%), and V_2O_5 (Alfa Aesar, 99.6%).

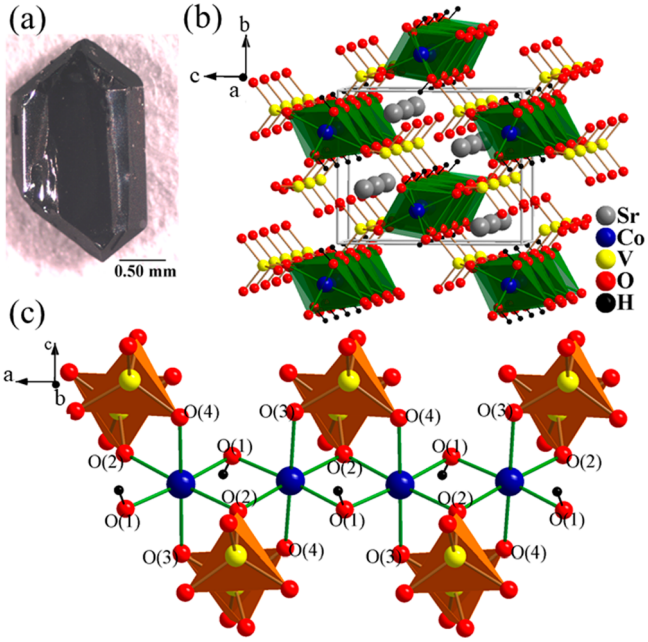

Figure 1. (a) Hydrothermally grown single crystal of $SrCo(VO_4)(OH)$. (b) View of $SrCo(VO_4)(OH)$ projected along the a-axis, showing packing of Co−O−Co chains along the b−c plane. The Sr^{2+} ions reside between the channels made from CoO_6 octahedra (green polyhedra) and VO_4 tetrahedra. (c) Partial structure of Co−O−Co chains made from edge-sharing CoO_6 octahedra along the a-axis. The VO_4 tetrahedra (orange polyhedra) connect with Co−O−Co chains in an up and down fashion along the chain. Hydrogen atoms connect to O(1) forming the only OH group in the structure.

2.2. X-ray Diffraction. Crystals of $SrCo(VO_4)(OH)$ were physically examined and selected under an optical microscope equipped with a polarizing attachment. The crystals of $SrCo(VO_4)(OH)$ were mounted on a glass fiber with epoxy. Room-temperature single-crystal X-ray diffraction data were collected using a four-circle Rigaku AFC8 diffractometer equipped with a Mercury CCD area detector, with Mo Kα (λ = 0.71073 Å) radiation. Data collection, processing, and scaling were performed using CrystalClear software suites.[30] The structures were determined by direct methods and refined by full-matrix least squares on $F2$ using the SHELXTL software suite.[31] All non-hydrogen atoms were refined anisotropically. In the case of the OH group, hydrogen atom positions were identified from the difference electron density map, and their occupancies were set to conform to realistic geometries in accord with electroneutrality requirements. Table 1 provides the detailed unit cell parameters with selected bond distances in Table 2. In addition, crystallographic orientations were also determined using the single-crystal X-ray diffractometer.

2.3. Characterization of Magnetic Properties. Temperature-dependent and field-dependent magnetic measurements were

DOI: 10.1021/acs.inorgchem.9b02427
Inorg. Chem. XXXX, XXX, XXX−XXX

Table 1. Crystallographic Data of $SrCo(VO_4)(OH)$ Determined by Single-Crystal X-ray Diffraction

empirical formula	$SrCo(VO_4)(OH)$
formula weight (g/mol)	278.50
crystal system	orthorhombic
crystal dimensions (mm)	0.16 × 0.10 × 0.08
space group, Z	$P2_12_12_1$ (No. 19), 4
T (K)	298
a (Å)	6.0157(2)
b (Å)	7.645(2)
c (Å)	9.291(3)
volume (Å^3)	427.30(2)
D(calc) (g/cm^3)	4.329
μ (Mo Kα) (mm^{-1})	18.323
F(000)	516
T_{max}, T_{min}	1.0000, 0.5158
2θ range (deg)	3.382−26.050
no. of reflections collected	3953
data/restraints/parameters	844/1/79
final R values [$I > 2\sigma(I)$] (R_1, R_{w2})	0.0253, 0.0586
final R values (all data) (R_1, R_{w2})	0.0239, 0.0578
goodness of fit	1.107
largest difference peak/hole (e/Å^3)	0.0696/−0.832
Flack parameter	0.38(2)

Table 2. Selected Bond Distances (angstroms) and Angles (degrees) of $SrCo(VO_4)(OH)$

$Co(1)O_6$	
Co(1)−O(1)	1.976(5)
Co(1)−O(1)	1.981(6)
Co(1)−O(2)	2.147(5)
Co(1)−O(2)	2.222(5)
Co(1)−O(3)	2.183(6)
Co(1)−O(4)	2.198(5)
$V(1)O_4$	
V(1)−O(2)	1.734(5)
V(1)−O(3)	1.730(5)
V(1)−O(4)	1.718(5)
V(1)−O(5)	1.687(5)
Co(1)−O(1)−Co(1)	99.08(3)
Co(1)−O(2)−Co(1)	87.13(3)
Co···Co	3.011(3)

performed using a Quantum Design Magnetic Property Measurement System (MPMS). Here, the single-crystal specimen was affixed to a quartz rod using GE varnish, and the magnetic properties perpendicular to the flat surface of the single crystal were determined by sandwiching the single crystal between two quartz rods. The temperature-dependent magnetization measurements were carried out along all three crystallographic directions from 2 to 300 K in applied magnetic fields of 10 and 40 kOe. Similarly, isothermal magnetization measurements were performed at 2, 50, and 300 K at magnetic fields of ≤50 kOe. Heat capacity measurements of $SrCo(VO_4)(OH)$ were performed using the Physical Property Measurement System (PPMS, Quantum Design) in applied magnetic fields of 0 and 40 kOe.

2.4. Neutron Scattering. Single-crystal neutron diffraction data were collected using the HB3A four-circle diffractometer at the High Flux Isotope Reactor at Oak Ridge National Laboratory.[32] For data collection, a single crystal of $SrCo(VO_4)(OH)$ was glued to an aluminum pin and loaded into a closed-cycle refrigerator that provides sample temperature control within the window of 4−300 K. A wavelength of 1.542 Å was selected by a Si-220 monochromator.

3. RESULTS AND DISCUSSION

3.1. Crystal Structure of $SrCo(VO_4)(OH)$. $SrCo(VO_4)(OH)$ crystallizes in an orthorhombic crystal system in space group $P2_12_12_1$ (No. 19). The room-temperature unit cell parameters are as follows: a = 6.0157(15) Å, b = 7.645(2) Å, c = 9.291(3) Å, and V = 427.30(2) Å^3. Significant crystallographic parameters, bond distances, and angles are summarized in Tables 1 and 2, respectively. The detailed crystallographic data, including Wyckoff positions and thermal parameters, are listed in Table S1. The material is isostructural with $SrMn(VO_4)(OH)$-descloizite. A detailed structural discussion of $SrCo(VO_4)(OH)$ (given below) is important for the understanding of the magnetic structure compared to $SrMn(VO_4)(OH)$. The structure is comprised of individual crystallographically independent Sr^{2+}, Co^{2+}, and V^{5+} sites. The Co^{2+} ions form distorted octahedra forming edge-shared one-dimensional (1D) Co−O−Co chains along the a-axis (Figure 1b,c). The VO_4 tetrahedra connect the 1D Co−O−Co chains to each other along the b−c plane imparting a three-dimensional nature onto $SrCo(VO_4)(OH)$. The Co−O bond lengths vary from 1.976(5) to 2.222(5) Å, highlighting the distortion in the CoO_6 octahedra, while the O−Co−O bond angles vary from 85.8(2)° to 97.1(4)°. The CoO_6 units are interconnected via O(1) and O(2) sharing edges. It is noteworthy that Co−O(1) and Co−O(2) form the shortest and longest Co−O bonds within the CoO_6 octahedra, respectively (Figure 1c). The edge-sharing O(1) atoms are also bound to H, generating the OH group in the structure. The other oxygen atoms [O(2)−O(4)] connect with VO_4 tetrahedral groups in an up and down fashion along the cobalt oxide chains (Figure 1c). Each VO_4 tetrahedral group shares edges with one Co−O−Co chain via O(3) and O(4) and is corner-shared with another Co−O−Co chain via O(2) along the b−c plane (Figure 1c). The V−O bond lengths in the VO_4 tetrahedra range from 1.687(5) to 1.718(5) Å.

Because V^{5+} is nonmagnetic, the VO_4 groups generate structurally confined 1D Co−O−Co chains along the a-axis. However, interchain interactions are possible via the Co−O−V−O−Co connectivity. Figure 2 highlights the distance between Co^{2+} sites within the chain, which is 3.011(3) Å, while the shortest interchain cobalt−cobalt distance is 5.951(5) Å. In addition, the Co−O(1)−Co and Co−O(2)−Co bond angles are 87.13(3)° and 99.08(3)°, respectively. Compared to those of $SrMn(VO_4)(OH)$, the M−O−M angles are slightly larger in $SrCo(VO_4)(OH)$ [Mn−O−Mn bond angles of 86.68(8)° and 96.69(9)°], while the intrachain metal−metal distance is very similar. Additionally, the shortest interchain Mn−Mn distance in $SrMn(VO_4)(OH)$ is 6.004(3) Å. These subtle structural changes and the different spin state lead to different magnetic properties for $SrCo(VO_4)(OH)$ compared to those of the manganese analogue.

3.2. Magnetic Properties of $SrCo(VO_4)(OH)$. The magnetic properties of $SrCo(VO_4)(OH)$ were examined by magnetic susceptibility (field cooling mode), isothermal magnetization, and heat capacity. Both the magnetic susceptibility and the isothermal magnetization were examined in three crystallographic directions. Figure 3 shows the magnetic susceptibility measured at an applied magnetic field of 10 kOe along the a-, b-, and c-axes. The magnetic susceptibility along the a-axis, which is the Co−O−Co chain direction, sharply rises with a decrease in temperature, reaching a maximum at 10 K, and then decreases rapidly, suggesting

DOI: 10.1021/acs.inorgchem.9b02427
Inorg. Chem. XXXX, XXX, XXX−XXX

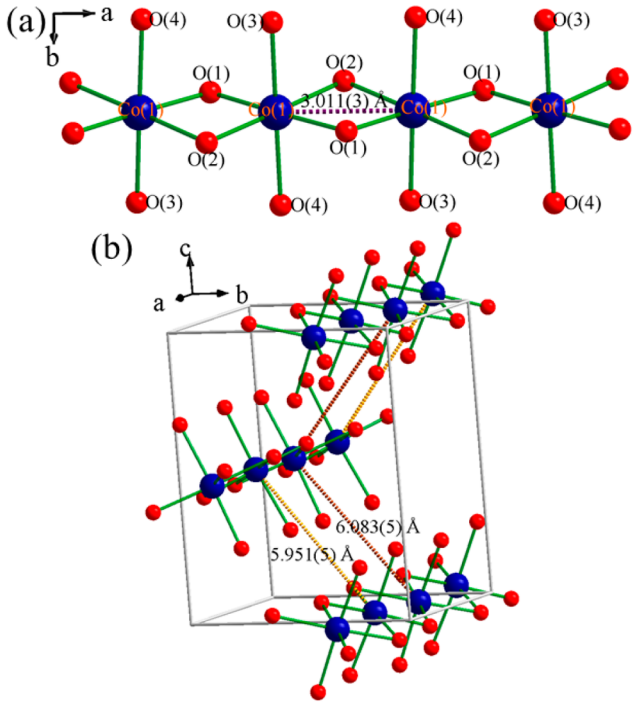

Figure 2. (a) Fragment of the Co−O−Co chain along the *a*-axis showing the edge-sharing connectivity of the CoO_6 octahedra. The intrachain distance between two Co atoms is highlighted by a purple dotted line [3.011(3) Å]. (b) Interchain distances highlighted with orange dotted lines. The shortest distance between the chains is 5.951(5) Å.

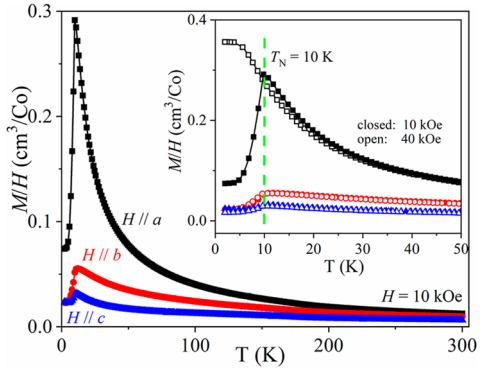

Figure 3. Susceptibility data of $SrCo(VO_4)(OH)$ measured at 10 kOe along three different crystallographic axes. The inset shows a comparison of susceptibility data at 10 and 40 kOe (empty symbols) in all three crystallographic directions. Susceptibility along the chain axis shows a significant difference with the applied magnetic field (all data collected in field cooling mode).

antiferromagnetic ordering at T_N = 10 K. Compared to the *a*-direction, the susceptibility along other two crystallographic directions does not exhibit a sharp increase with a decrease in temperature, indicating a strong anisotropy, with the magnetic easy axis oriented along the chain direction. A significant anisotropic behavior of the susceptibility curves was observed even in the paramagnetic regime. Similar behavior has been observed in $BaCo_2V_2O_8$ and CoV_2O_6, which contain 1D Co^{2+} edge-shared octahedral chains like the compound in this study. This behavior could be attributed to the large single-ion anisotropy due to spin orbit coupling of Co^{2+} and to the quasi 1D nature of the magnetic interactions.[32,33] The inset of Figure 3 shows the magnetization as a function of applied magnetic fields of 10 and 40 kOe in all three crystallographic directions. Here, 10 and 40 kOe temperature-dependent magnetic susceptibility data along the *b*- and *c*-directions almost overlap with each other, indicating no field-dependent susceptibility. However, when the applied magnetic field is oriented along the *a*-direction, in the higher field the magnetic susceptibility continuously increases without showing a peak at 10 K. This indicates a field-induced magnetic transition along the chain direction. The magnetic susceptibility measured in a 10 kOe field was used for Curie−Weiss fits. The Curie−Weiss fits were performed for all three crystallographic directions using the data between 200 and 300 K. The fits produced Θ_{CW} values of 8, −47, and −181 K along the *a*-, *b*-, and *c*-axes, respectively. Additionally, effective magnetic moments in the three different directions are 5.4, 5.2, and 4.9 μ_B, respectively. These values are higher than the spin only value of Co^{2+} with $S = {}^3/_2$ and μ_{eff} = 3.8 μ_B. This could be due to the significant orbital contribution because orbital moments are unquenched for Co^{2+} in an octahedral environment ($t_{2g}{}^5e_g{}^2$, $S = {}^3/_2$, L = 3). Similar higher values have been observed previously for 1D Co^{2+}-chain compounds such as CoV_2O_6 (saturated moment of 4.4 μ_B), $BaCo_2V_2O_8$ (5.20 μ_B), $CoSe_2O_5$ (5.20 μ_B), Na_4CoTeO_6 (5.14 μ_B), and $NaCoSO_4F$ (5.20 μ_B).[32−38] In addition, effective magnetic moments in all three crystallographic directions do not deviate largely from each other. In contrast, a large deviation was observed in the Curie−Weiss temperatures. Therefore, we fitted the average magnetic susceptibility data obtained by averaging the magnetic susceptibilities along all three crystallographic directions. The fitted Θ_{CW} and effective magnetic moments are −36 K and 5.05 μ_B, respectively, which further confirms the dominant antiferromagnetic interactions of $SrCo(VO_4)(OH)$.[33,34,37]

Figure 4 displays the isothermal magnetization of $SrCo(VO_4)(OH)$ measured along three different crystallographic directions. The data were collected at 2−50 K. Below the T_N, a significant field dependence was observed in all three directions. An extremely sharp upturn (metamagnetic transition) was observed along the *a*-direction, which is the Co−O−Co chain direction. This metamagnetic transition along the *a*-direction occurs at approximately 27 kOe and could be due to the spin rearrangement from an antiferromagnetic ground state to a ferromagnetic state. This behavior agrees well with our magnetic susceptibility data observed along the *a*-axis. Additionally, the change in magnetization [ΔM (H = 0)] at the field-induced transition is ∼2 μ_B/Co, which further agrees with our refined magnetic moment projections obtained from our neutron diffraction data (see discussion below). Above the metamagnetic transition, the magnetization continuously rises, approaching 2.7 μ_B/Co at 70 kOe. At the same time, isothermal magnetizations measured at other two directions below 10 K (T_N) do not show steep transitions; however, there is a slight curvature associated with each. This suggests that Co spins rotate toward the *a*-axis by producing a ferromagnetic state. It is worth noting that the overall magnetism observed in $SrCo(VO_4)(OH)$ is very similar to that of CoV_2O_6; both compounds have a 1D Co−O−Co chain made from highly distorted $Co^{2+}O_6$ octahedra.[32] In CoV_2O_6, a large difference in magnetic susceptibility was observed in different crystallographic directions (the *c*-axis is the magnetic easy axis) even at room temperature. In addition, isothermal magnetization measured at 5 K exhibits a staircase magnetization curve

DOI: 10.1021/acs.inorgchem.9b02427
Inorg. Chem. XXXX, XXX, XXX−XXX

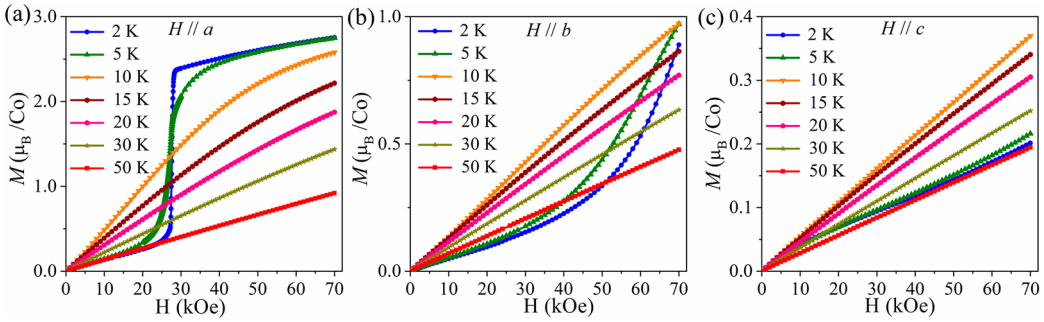

Figure 4. Field-dependent data obtained by applying a magnetic field along the *a*-, *b*-, and *c*-axes. A sharp metamagnetic transition was observed along the *a*-axis at 27 kOe with a slight curvature observed along the other two axes at 2 K.

along the Co−O−Co chain direction (*c*-axis) and a linear behavior in the other two directions (*a*- and *b*-axes). A first jump in isothermal magnetization along the *c*-axis was observed at 16 kOe, reaching to 1.4 μ_B/Co, followed by a second jump at 33 kOe and a saturation of magnetization to 4.4 μ_B/Co at ∼40 kOe. The saturated magnetic moment is much larger than the spin only value of Co^{2+} (3 μ_B/Co) that was described as an indication of a large orbital contribution from the distorted CoO_6 oxygen environment.[32]

Heat capacity (C_p) measurements of $SrCo(VO_4)(OH)$ were performed between 30 and 2 K at zero applied magnetic field and a 40 kOe applied magnetic field. The results are shown in Figure 5. Here field was applied along the *c*-axis of the single

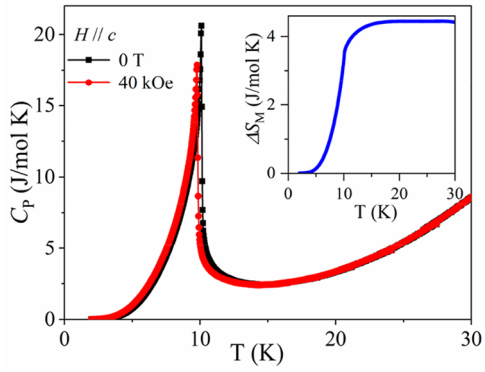

Figure 5. Heat capacity measured at *H* values of 0 and 40 kOe exhibiting a sharp anomaly at the magnetic ordering temperature. The inset shows the magnetic entropy of $SrCo(VO_4)(OH)$.

crystal. A zero field heat capacity displays a sharp peak at 10 K that corresponds to the T_N observed in magnetic susceptibility. There is a small effect from applying the 40 kOe field along the *c*-axis with a 0.3 K shift to the lower temperature, which is consistent with magnetization data, and this could be due to a small reorientation of the spin axis.[35] To calculate the magnetic entropy, the heat capacity data of $SrCo(VO_4)(OH)$ above 15 K were fitted by the equation $C_p = \gamma T + \beta_1 T^3 + \beta_1 T^5 + \beta_1 T^7$, where $\gamma = 0$ for an insulator and $\beta_1 T^3 + \beta_1 T^5 + \beta_1 T^7$ is the contribution from the lattice (C_l). Therefore, the magnetic contribution, C_m, was calculated as the difference $C_p - C_l$. The magnetic entropy, S_M, was estimated by integrating $C_{mag}/T\ dT$. As shown in the inset of Figure 5, the calculated magnetic entropy (S_M) is 4.43 J mol^{-1} K^{-1}. The expected entropy (ΔS) for Co^{2+} in the $S = {}^3/_2$ spin state is 11.5 J mol^{-1} K^{-1} [$\Delta S = R \ln(2S + 1)$], and the observed magnetic entropy is 38% from $R \ln(2S + 1)$. This difference could be attributed to the highly anisotropic behavior that we observed in magnetic susceptibility. In addition, a relatively smaller magnetic entropy has been observed in 1D compounds such as $CoSe_2O_5$, $Pb_2Co(V_2O_7)(OH)Cl$, and $SrMn(VO_4)(OH)$.[19,35,39]

3.3. Magnetic Structure of $SrCo(VO_4)(OH)$. Single-crystal neutron diffraction data were collected at two different temperatures, 15 and 4 K, above and below T_N. The magnetic structure was determined by modeling the intensities of magnetic Bragg peaks measured below the ordering temperature. A survey of the reciprocal lattice at 4 K revealed a magnetic order with the propagation vector **k** = (0, 0, 0). Thus, the magnetic unit cell is of the same size as the chemical cell, and the intensities measured at 4 K contain both nuclear and magnetic scattering contributions. A systematic search for magnetic models was carried out using the subtracted intensities (4 K − 15 K) that allowed separation of the magnetic and nuclear scattering, on a set of 34 unique reflections. Ultimately, refinements were carried out using a combined structural and magnetic model using the 4 K data. The extinction coefficients and thermal parameters were fixed to the values obtained from the paramagnetic state, measured at 15 K. The refined structural parameters at both 15 and 4 K are similar to those obtained from the X-ray data, listed in Table 1. To understand further the magnetic ordering temperature, order parameters were determined by following the temperature dependence of the (001) Bragg peak. Figure 6 displays the order parameter curves, and it follows the power law indicating the onset of magnetic long-range ordering at 9.4 K, which is in good agreement with our magnetic susceptibility

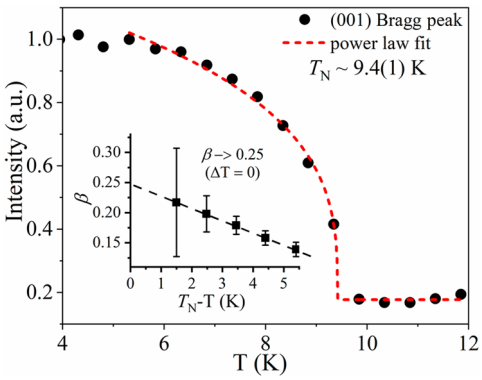

Figure 6. Temperature dependence of the (001) Bragg peak intensity and the fit using the power-law model as described in the text. The inset shows the critical exponent β associated with the magnetic order parameter as a function of fitting range (ΔT).

DOI: 10.1021/acs.inorgchem.9b02427
Inorg. Chem. XXXX, XXX, XXX−XXX

and heat capacity data. The power-law equation used for fitting the order parameter data is $I \propto m(T)^2 \propto (T_N - T)^{2\beta}$, and we found that β approaches 0.25 for $\Delta T \rightarrow 0$, which is close to the expected value for the 2D-XY model ($\beta \sim 0.23$) expected for layered magnetic structures.[40]

Representational theory and magnetic symmetry analysis have been employed to determine the symmetry-allowed magnetic structure models, derived from the crystal $P2_12_12_1$ symmetry and the wave vector **k** = (0, 0, 0). Calculations were carried out using the program SARAh Representational Analysis[41] and the MAXMAGN program available at the Bilbao Crystallographic Server.[42] The possible maximal magnetic space groups for the parent space group $P2_12_12_1$ and the propagation vector **k** = (0, 0, 0) are summarized in Table 3. The best fit to the data is obtained using the magnetic space group $P2_12_12_1$, which enables ferromagnetic spin orientation inside the chain and antiferromagnetic alignment between chains. The Wyckoff positions and the associated magnetic moments are Co1: (0.254, 0.243, 0.495|m_a, m_b, m_c), Co2: (0.245, 0.757, 0.995|$-m_a$, $-m_b$, m_c), Co3: (0.745, 0.743, 0.005|$-m_a$, m_b, $-m_c$), and Co4: (0.755, 0.257, 0.505|m_a, $-m_b$, $-m_c$). This spin configuration is different from that found in the case of the Mn compound, where the magnetic order was described by the monoclinic $P2_1$ magnetic space group that allowed the existence of an uncompensated ferromagnetic component along the *a*-axis. The canted structure was thought to be due to antisymmetric Dzyaloshinskii–Moriya (DM) interactions, which arise from the broken inversion symmetry in $SrMn(VO_4)(OH)$. Interestingly, no symmetry lowering is required for the magnetic ordering in $SrCo(VO_4)(OH)$. In the latter, the magnetic moments are canted ($45 \pm 3°$) and follow rigidly the staggered rotation of CoO_6 octahedra, likely due to spin–orbit coupling. The spins are oriented along the shortest basal bond, Co–O(1), but the canting follows opposite directions along adjacent chains. The refined moment projections are m_a = 2.1(1) μ_B, m_b = 2.1(1) μ_B, and m_c = 0.6(1) μ_B. The total Co ordered moment is 3.0(2) μ_B, which is consistent with that expected for $S = {}^3/_2$. The proposed magnetic structure model is depicted in Figure 7, in the form of two distinct projections along the *c*- and *a*-axes. We note that a comparable canted spin arrangement was reported for $NaCoSO_4F$.[38] The spin orientation was associated with the strong magnetocrystalline anisotropy of the Co^{2+} ion, which results from the relatively strong spin–orbit coupling.

Table 3. Maximal Magnetic Space Groups and Associated Wyckoff Positions and Magnetic Moments for the Parent Space Group $P2_12_12_1$ and the Propagation Vector k = (0, 0, 0)[a]

Magn. SG	Transformation matrix	Wyckoff positions and Magnetic Moments
$P2_12_12_1$ (#19.25)	$\begin{pmatrix}1&0&0&0\\0&1&0&0\\0&0&1&0\end{pmatrix}$	x,y,z | m_a,m_b,m_c); (-x+1/2,-y,z+1/2 | -m_a,-m_b,m_c) (-x,y+1/2,-z+1/2 | -m_a,m_b,-m_c) (x+1/2,-y+1/2,-z | m_a,-m_b,-m_c)
$P2_1'2_12_1$ (#19.27)	$\begin{pmatrix}1&0&0&0\\0&1&0&0\\0&0&1&0\end{pmatrix}$	(x,y,z | m_a,m_b,m_c) (-x+1/2,-y,z+1/2 | -m_a,-m_b,m_c) (-x,y+1/2,-z+1/2 | m_a,-m_b,m_c) (x+1/2,-y+1/2,-z | -m_a,m_b,m_c)
$P2_12_1'2_1$ (#19.27)	$\begin{pmatrix}1&0&0&1/4\\0&0&-1&1/4\\0&1&0&1/4\end{pmatrix}$	(x,y,z | m_a,m_b,m_c) (-x+1/2,-y,z+1/2 | m_a,m_b,-m_c) (-x,y+1/2,-z+1/2 | -m_a,m_b,-m_c) (x+1/2,-y+1/2,-z | -m_x,m_b,m_c)
$P2_12_12_1'$ (#19.27)	$\begin{pmatrix}0&0&1&1/4\\0&1&0&1/4\\-1&0&0&1/4\end{pmatrix}$	(x,y,z | m_a,m_b,m_c) (-x+1/2,-y,z+1/2 | m_a,m_b,-m_c) (-x,y+1/2,-z+1/2 | m_a,-m_b,m_c) (x+1/2,-y+1/2,-z | m_a,-m_b,-m_c)

[a]The four equivalent Co positions are defined as Co1: (0.254, 0.243, 0.495), Co2: (0.245, 0.757, 0.995), Co3: (0.745, 0.743, 0.005), and Co4: (0.755, 0.257, 0.505).

3.4. Magnetic Transitions in $SrCo(VO_4)(OH)$. We now discuss the phenomenological theory of the magnetization observed in $SrCo(VO_4)(OH)$. The $SrCo(VO_4)OH$ system consists of $S = {}^3/_2$ Co(II) chains that exhibit strong magnetocrystalline anisotropy along the orbitals approximately 45° from each chain. The zero-field ground state is shown in Figure 8a, where neighboring chains are coupled antiferromagnetically by $J_2 < 0$. Spins along each *a*-axis chain are

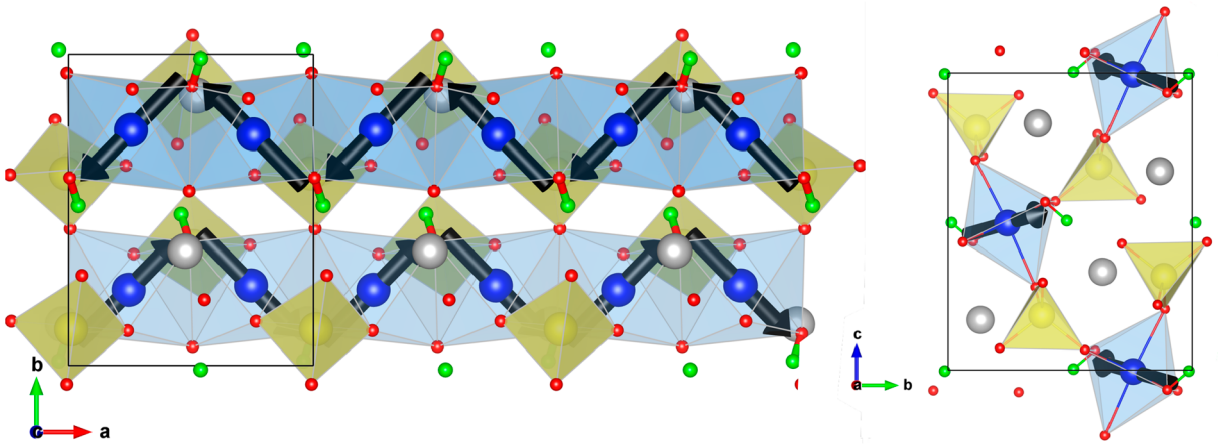

Figure 7. Magnetic structure of $SrCo(VO_4)(OH)$ at 4 K and zero field. The left panel shows the view along the *c*-axis, while the right panel presents a view along the *a*-axis (chain direction). The magnetic spins are arranged in a staggered configuration with a ferromagnetic alignment along the chain and an antiferromagnetic alignment between chains, producing a fully compensated AFM ordered state.

DOI: 10.1021/acs.inorgchem.9b02427
Inorg. Chem. XXXX, XXX, XXX–XXX

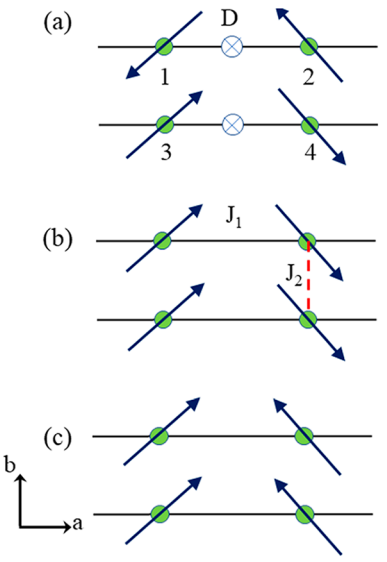

Figure 8. Three magnetic phases of $SrCo(VO_4)(OH)$. (a) Phase i is stable at zero field, and phases (b) ii and (c) iii are stable above critical field H_{ca} and H_{cb} for fields along the *a*- and *b*-axes, respectively.

coupled ferromagnetically by $J_1 > 0$. Strong orbital anisotropy is taken along the $\mathbf{n}_1 = (1, 1, 0)/\sqrt{2}$ and $\mathbf{n}_2 = (1, -1, 0)/\sqrt{2}$ directions with single-ion anisotropy constant K. Moreover, experimentally, the anisotropy K is much larger than the exchange J_1 because the spins are close to the orbital directions. This could be due to strong spin−orbit coupling. As allowed by the broken inversion symmetry around each Co−Co bond in the chain, we include alternating Dzyalloshinskii−Moriya (DM) interactions between neighboring spins in the chain with a constant D.

With four spins in the unit cell, the energy E per unit cell is given by

$$\begin{aligned} E/N = &-2J_1\{S_1\cdot S_2\cdot S_3\cdot S_4\} - 4J_2\{S_1\cdot S_3 + S_2\cdot S_4\} \\ &- K\{(S_1\cdot n_1)^2 + (S_2\cdot n_2)^2 + (S_3\cdot n_1)^2 + (S_4\cdot n_2)^2\} \\ &+ 2Dc\cdot\{(S_1 \times S_2) + (S_3 \times S_4)\} \\ &- 2\mu_B Hm\cdot\{S_1 + S_2 + S_3 + S_4\} \end{aligned}$$

where N is the number of unit cells. The factor of 4 in front of J_2 reflects the four neighboring chains. A magnetic field H is taken to lie along direction m. For the sake of simplicity, we ignore the small components of the spins along c.

If the anisotropy K is much larger than the exchange and DM interactions, then the spins can be considered to lie along the $\mathbf{n}_1$ or $\mathbf{n}_2$ directions. Hence, the zero-field ground-state energy per unit cell is given by

$$E_i/N = 8J_2S^2 - 4DS^2 - 4KS^2$$

Now consider the energies of $SrCo(VO_4)(OH)$ in magnetic fields along the *a*- or *b*-axis. Above the critical fields H_{ca} and H_{cb}, the spin configurations are pictured in panels b and c of Figure 8 with energies

$$E_{ii}/N = -8J_2S^2 - 4DS^2 - 4KS^2 - 4\sqrt{2\mu_B HS},$$

$$E_{iii}/N = -8J_2S^2 + 4DS^2 - 4KS^2 - 4\sqrt{2\mu_B HS}$$

In all cases, the nearest neighbor exchange energy proportional to J_1 vanishes because neighboring spins are perpendicular.

Setting $E_{ii} = E_i$ or $E_{iii} = E_i$, the critical fields are

$$H_{ca} = 2\sqrt{2|J_2|S/\mu_B},$$

$$H_{cb} = 2\sqrt{2|J_2|S/\mu_B} + \sqrt{2DS/\mu_B}$$

$$= H_{ca} + \sqrt{2DS/\mu_B}$$

Using the experimental result $H_{ca} = 2.7$ T, we estimate that $|J_2| \approx 0.037$ meV. Because $H_{cb} > 7$ T, we conclude that $D > 0.12$ meV. The magnetization induced by the field along the *a*- or *b*-axis below these critical fields reflects the fact that K is not infinite. So this magnetization is proportional to small contributions in the order $|J_2|/K$, J_1/K, and D/K. The components of the spin along the *c*-axis may also contribute below the critical fields.

4. CONCLUSIONS

Single crystals of $SrCo(VO_4)(OH)$ were synthesized using the high-temperature, high-pressure hydrothermal method. The structure of $SrCo(VO_4)(OH)$ is another addition to the adelite−descloizite mineral family that contains a Co^{2+} $S = {}^3/_2$ quasi one-dimensional magnetic chain. These chains are connected with each other via nonmagnetic tetrahedral vanadate groups. The single-crystal structure was determined using the X-ray single-crystal diffraction technique and confirms that $SrCo(VO_4)(OH)$ crystallizes in the noncentrosymmetric $P2_12_12_1$ space group. The high-temperature, high-pressure hydrothermal method allowed us to grow larger single crystals that can be used to determine the magnetic structure using single-crystal X-ray diffraction. The macroscopic magnetic measurements indicate a long-range magnetic ordering below $T_N = 10$ K with strong anisotropy along the *a*-axis, which is the Co^{2+}-chain axis. The isothermal magnetization data along the *a*-axis exhibit a metamagnetic-type transition at ∼27 kOe. We noted that the magnetic properties of $SrCo(VO_4)(OH)$ are different from those of the isostructural $SrMn(VO_4)(OH)$ compound. This could be due to the stronger spin−orbit couplings present in Co^{2+} and the subtle structural difference associated with the slightly smaller unit cell of $SrCo(VO_4)(OH)$ compared to that of $SrMn(VO_4)(OH)$, which eventually can affect the interchain interactions. Single-crystal neutron diffraction data revealed a magnetic structure that consists of ferromagnetic chains that are coupled antiferromagnetically. Inside the chains, the Co moments are canted to follow the staggered rotation of CoO_6 octahedra and maintain the orientation along the shortest basal bond Co−O(1). An applied magnetic field along the chain direction induces a spin realignment that likely results in an order in which the spin-canting direction is identical in all of the chains. Additionally, a phenomenological model was introduced to describe the magnetic ground state at zero applied magnetic field and the field-induced magnetic ground state. A very small but finite DM interaction between next nearest Co within the chain along the *a*-axis was essential for describing the metamagnetic transition. The physical properties of this $SrM(VO_4)(OH)$ (M = Mn and Co) series suggest that complex intrachain and interchain interactions are possible and provide a fertile ground for investigating the interplay among the various magnetic ions inherited in the isostructures.

DOI: 10.1021/acs.inorgchem.9b02427
Inorg. Chem. XXXX, XXX, XXX−XXX

Finally, inelastic neutron scattering experiments are essential for evaluating the spin Hamiltonian of $SrM(VO_4)(OH)$ series in further detail.

■ ASSOCIATED CONTENT

Supporting Information

The Supporting Information is available free of charge at https://pubs.acs.org/doi/10.1021/acs.inorgchem.9b02427.

Crystallographic refinement data from single-crystal X-ray diffraction of $SrCo(VO_4)(OH)$ (PDF)

Accession Codes

CCDC 1944736 contains the supplementary crystallographic data for this paper. These data can be obtained free of charge via www.ccdc.cam.ac.uk/data_request/cif, or by emailing data_request@ccdc.cam.ac.uk, or by contacting The Cambridge Crystallographic Data Centre, 12 Union Road, Cambridge CB2 1EZ, UK; fax: +44 1223 336033.

■ AUTHOR INFORMATION

Corresponding Authors

*E-mail: sanjeewald@ornl.gov.
*E-mail: kjoseph@clemson.edu.

ORCID

Liurukara D. Sanjeewa: 0000-0002-3293-7370
Michael A. McGuire: 0000-0003-1762-9406

Notes

The authors declare no competing financial interest.

■ ACKNOWLEDGMENTS

This work was primarily performed at the Oak Ridge National Laboratory Materials Sciences and Technology Division (physical property measurements) and Scientific User Facilities Division (neutron scattering) funded by the U.S. Department of Energy, Office of Science, Basic Energy Sciences. The synthesis and single-crystal X-ray diffraction were performed at Clemson University and funded by the National Science Foundation under Grant DMR-1410727.

■ REFERENCES

(1) Giamarchi, T. *Quantum Physics in One Dimension*; Oxford University Press Inc.: New York, 2003.
(2) Balents, L. Spin Liquids in Frustrated Magnets. *Nature* **2010**, *464*, 199−208.
(3) Vasil'ev, A. N.; Markina, M. M.; Popova, E. A. Spin Gap in Lowdimensional Magnets. *Low Temp. Phys.* **2005**, *31*, 203−223.
(4) Hase, M.; Terasaki, I.; Uchinokura, K. Observation of the Spin Peierls Transition in Linear (Spin-1/2) Chains in an Inorganic compound $CuGeO_3$. *Phys. Rev. Lett.* **1993**, *70*, 3651−3654.
(5) He, Z.; Kyômen, T.; Itoh, M. Quasi-one-dimensional Alternating Chain Compound with a Large Spin Gap $BaCu_2V_2O_8$. *Phys. Rev. B: Condens. Matter Mater. Phys.* **2004**, *69*, 220407.
(6) Garrett, A. W.; Nagler, S. E.; Tennant, D. A.; Sales, B. C.; Barnes, T. Magnetic Excitations in the Alternating Chain Compound $(VO)_2(P_2O_7)$. *Phys. Rev. Lett.* **1997**, *79*, 745−748.
(7) Ueda, Y. Vanadate Family as Spin-Gap Systems. *Chem. Mater.* **1998**, *10*, 2653−2664.
(8) Kaul, E. E.; Rosner, H.; Yushankhai, V.; Sichelschmidt, J.; Shpanchenko, R. V.; Geibel, C. $Sr_2V_3O_9$ and $Ba_2V_3O_9$: Quasi-one-dimensional Spin-systems with an Anomalous Low Temperature Susceptibility. *Phys. Rev. B: Condens. Matter Mater. Phys.* **2003**, *67*, 174417.
(9) Sanjeewa, L. D.; McGuire, M. A.; Garlea, V. O.; Hu, L.; Chumanov, G.; McMillen, C. D.; Kolis, J. W. Hydrothermal Synthesis and Characterization of Novel Brackebuschite-Type Transition Metal Vanadates: $Ba_2M(VO_4)_2(OH)$, M = V^{3+}, Mn^{3+}, and Fe^{3+}, with Interesting Jahn-Teller and Spin-Liquid Behavior. *Inorg. Chem.* **2015**, *54*, 7014−7020.
(10) Cheng, J.; Tian, W.; Zhou, J.; Lynch, V. M.; Steinfink, H.; Manthiram, A.; May, A. F.; Garlea, V. O.; Neuefeind, J. O.; Yan, J. Crystal and Magnetic Structures and Physical Properties of a New Pyroxene $NaMnGe_2O_6$ Synthesized Under High Pressure. *J. Am. Chem. Soc.* **2013**, *135*, 2776−2786.
(11) He, Z.; Taniyama, T.; Kyômen, T.; Itoh, M. Field-induced Order-disorder Transition in the Quasi-one-dimensional Anisotropic Antiferromagnet $BaCo_2V_2O_8$. *Phys. Rev. B: Condens. Matter Mater. Phys.* **2005**, *72*, 172403.
(12) Garlea, V. O.; Sanjeewa, L. D.; McGuire, M. A.; Kumar, P.; Sulejmanovic, D.; He, J.; Hwu, S.-J. Complex Magnetic Behavior of the Sawtooth Fe Chains in $Rb_2Fe_2O(AsO_4)$. *Phys. Rev. B: Condens. Matter Mater. Phys.* **2014**, *89*, 014426.
(13) McMillen, C. D.; Kolis, J. W. Hydrothermal Synthesis as a Route to Mineralogically-Inspired Structures. *Dalton Trans.* **2016**, *45*, 2772−2784.
(14) Streltsov, S. V.; Khomskii, D. I. Electronic Structure and Magnetic Properties of Pyroxenes (Li, Na)TM(Si, Ge)$_2O_6$: Low-dimensional Magnets with 90° Bonds. *Phys. Rev. B: Condens. Matter Mater. Phys.* **2008**, *77*, 064405.
(15) Millet, P.; Mila, F.; Zhang, F. C.; Mambrini, M.; Van Oosten, A. B.; Pashchenko, V. A.; Sulpice, A.; Stepanov, A. Biquadratic Interactions and Spin-Peierls Transition in the Spin-1 Chain $LiVGe_2O_6$. *Phys. Rev. Lett.* **1999**, *83*, 4176.
(16) Zhang, S.; Xiang, H.; Guo, W.; Tang, Y.; Cui, M.; He, Z. Synthesis, Characterization, and Mechanism Analysis of S = 2 Quasi-One-Dimensional Ferromagnetic Semiconductor $Pb_2Mn(VO_4)_2(OH)$. *Dalton Trans.* **2016**, *45*, 7022−7027.
(17) Effenberger, H.; Krause, W.; Bernhardt, H. J. *Ninth International Symposium on Experimental Mineralogy, Petrology and Geochemistry*; Zurich, 2002; Vol. 9, p 30.
(18) Hawthorne, F. C.; Faggiani, R. Refinement of the Structure of Deseloizite. *Acta Crystallogr., Sect. B: Struct. Crystallogr. Cryst. Chem.* **1979**, *35*, 717.
(19) Sanjeewa, L. D.; Garlea, O. V.; McGuire, M. A.; McMillen, C. D.; Cao, H.; Kolis, J. W. Structural and Magnetic Characterization of the One-Dimensional S = 5/2 Antiferromagnetic Chain System $SrMn(VO_4)(OH)$. *Phys. Rev. B: Condens. Matter Mater. Phys.* **2016**, *93*, 224407.
(20) Garlea, V. O.; Sanjeewa, L. D.; McGuire, M. A.; Batista, C. D.; Samarakoon, A. M.; Graf, D.; Winn, B.; Ye, F.; Hoffmann, C.; Kolis, J. W. Exotic Magnetic Field-Induced Spin-Superstructures in a Mixed Honeycomb-Triangular Lattice System. *Phys. Rev. X* **2019**, *9*, 011038.
(21) Sanjeewa, L. D.; McMillen, C. D.; Willett, D.; Chumanov, G.; Kolis, J. W. Hydrothermal Synthesis of Single Crystals of Transition Metal Vanadates in the Glaserite Phase. *J. Solid State Chem.* **2016**, *236*, 61−68.
(22) Sanjeewa, L. D.; McMillen, C. D.; McGuire, M. A.; Kolis, J. W. Manganese Vanadate Chemistry in Hydrothermal BaF_2 Brines: $Ba_3Mn_2(V_2O_7)F_2$ and $Ba_7Mn_8O_2(VO_4)_2F_{23}$. *Inorg. Chem.* **2016**, *55*, 12512−12515.
(23) Sanjeewa, L. D.; McGuire, M. A.; McMillen, C. D.; Willett, D.; Chumanov, G.; Kolis, J. W. Honeycomb-like S = 5/2 Spin Lattices in New Manganese(II) Vanadates. *Inorg. Chem.* **2016**, *55*, 9240−9249.
(24) Taddei, K. M.; Sanjeewa, L. D.; Kolis, J. W.; Sefat, A. S.; de la Cruz, C.; Pajerowski, D. M. Local-Ising-Type Magnetic Order and Metamagnetism in the Rare-Earth Pyrogermanate $Er_2Ge_2O_7$. *Phys. Rev. Mater.* **2019**, *3*, 014405.
(25) Natarajan, S.; Mandal, S. Open-Framework Structures of Transition-Metal Compounds. *Angew. Chem., Int. Ed.* **2008**, *47*, 4798−4828.
(26) Hwu, S.-J. Structurally Confined Transition-Metal Oxide Layers, Chains and Oligomers in Molecular and Extended Magnetic Solids. *Chem. Mater.* **1998**, *10*, 2846−2859.

DOI: 10.1021/acs.inorgchem.9b02427
Inorg. Chem. XXXX, XXX, XXX−XXX

(27) Krivovichev, S. V. Which Inorganic Structures are the Most Complex? *Angew. Chem., Int. Ed.* **2014**, *53*, 654−661.
(28) Geertsma, W.; Khomskii, D. Influence of Side Groups on 90° Superexchange: A Modification of the Goodenough-Kanamori-Anderson Rules. *Phys. Rev. B: Condens. Matter Mater. Phys.* **1996**, *54*, 3011.
(29) *CrystalClear*; Rigaku and Molecular Structure Corp.: The Woodlands, TX, 2006.
(30) Sheldrick, G. M. A Short History of SHELX. *Acta Crystallogr., Sect. A: Found. Crystallogr.* **2008**, *64*, 112−122.
(31) Chakoumakos, B. C.; Cao, H. B.; Ye, F.; Stoica, A. D.; Popovici, M.; Sundaram, M.; Zhou, W.; Hicks, J. S.; Lynn, G. W.; Riedel, R. A. Four-circle Single-crystal Neutron Diffractometer at the High Flux Isotope Reactor. *J. Appl. Crystallogr.* **2011**, *44*, 655−658.
(32) He, Z.; Yamaura, J.-I.; Ueda, Y.; Cheng, W. CoV_2O_6 Single Crystals Grown in a Closed Crucible: Unusual Magnetic Behaviors with Large Anisotropy and 1/3 Magnetization Plateau. *J. Am. Chem. Soc.* **2009**, *131*, 7554−7555.
(33) He, Z.; Taniyama, T.; Itoh, M. Large Magnetic Anisotropy in the Quasi-one-dimensional System $BaCo_2V_2O_8$. *Appl. Phys. Lett.* **2006**, *88*, 132504.
(34) Rodriguez, E. E.; Cao, H.; Haiges, R.; Melot, B. C. Single Crystal Magnetic Structure and Susceptibility of $CoSe_2O_5$. *J. Solid State Chem.* **2016**, *236*, 39−44.
(35) Melot, B. C.; Paden, B.; Seshadri, R.; Suard, E.; Nenert, G.; Dixit, A.; Lawes, G. Magnetic Structure and Susceptibility of $CoSe_2O_5$: An Antiferromagnetic Chain Compound. *Phys. Rev. B: Condens. Matter Mater. Phys.* **2010**, *82*, 014411.
(36) He, Z.; Guo, W.; Cui, M.; Tang, Y. Synthesis and Magnetic Properties of New Tellurate Compounds Na_4MTeO_6 (M = Co and Ni) with a Ferromagnetic Spin-chain Structure. *Dalton Trans.* **2017**, *46*, 5076−5081.
(37) Bera, A. K.; Lake, B.; Stein, W. D.; Zander, S. Magnetic Correlations of the Quasi-one-dimensional Half-integer Spin-chain Antiferromagnets $SrM_2V_2O_8$ (M = Co, Mn). *Phys. Rev. B: Condens. Matter Mater. Phys.* **2014**, *89*, 094402.
(38) Melot, B. C.; Rousse, G.; Chotard, J.-N.; Kemei, M. C.; Rodriguez-Carvajal, J.; Tarascon, J.-M. Magnetic Structure and Properties of $NaFeSO_4F$ and $NaCoSO_4F$. *Phys. Rev. B: Condens. Matter Mater. Phys.* **2012**, *85*, 094415.
(39) Zhang, S.-Y.; Guo, W.-B.; Tang, Y.-Y.; Xu, J.-Q.; He, Z.-Z. Observation of Spin Relaxation in a Vanadate Chloride with QuasiOne-Dimensional Linear Chain. *Cryst. Growth Des.* **2019**, *19*, 2228−2234.
(40) Bramwell, S. T.; Holdsworth, P. C. W. Magnetization and Universal Sub-critical Behaviour in Two-dimensional XY Magnets. *J. Phys.: Condens. Matter* **1993**, *5*, L53.
(41) Wills, A. S. A New Protocol for the Determination of Magnetic Structures Using Simulated Annealing and Representational Analysis (SARA*h*). *Phys. B* **2000**, *276*−*278*, 680.
(42) Perez-Mato, J. M.; Gallego, S. V.; Tasci, E. S.; Elcoro, L.; de la Flor, G.; Aroyo, M. I. Symmetry-Based Computational Tools for Magnetic Crystallography. *Annu. Rev. Mater. Res.* **2015**, *45*, 217−248.

DOI: 10.1021/acs.inorgchem.9b02427
Inorg. Chem. XXXX, XXX, XXX−XXX